Assessment of synergistic interactions on self-assembled sodium alginate/ nano-hydroxyapatite composites: to the conception of new bone tissue dressings

Luciano Benedini, Damián Placente, Olga Pieroni & Paula Messina

Colloid and Polymer Science
Kolloid-Zeitschrift und Zeitschrift für Polymere

ISSN 0303-402X

Colloid Polym Sci
DOI 10.1007/s00396-017-4190-x

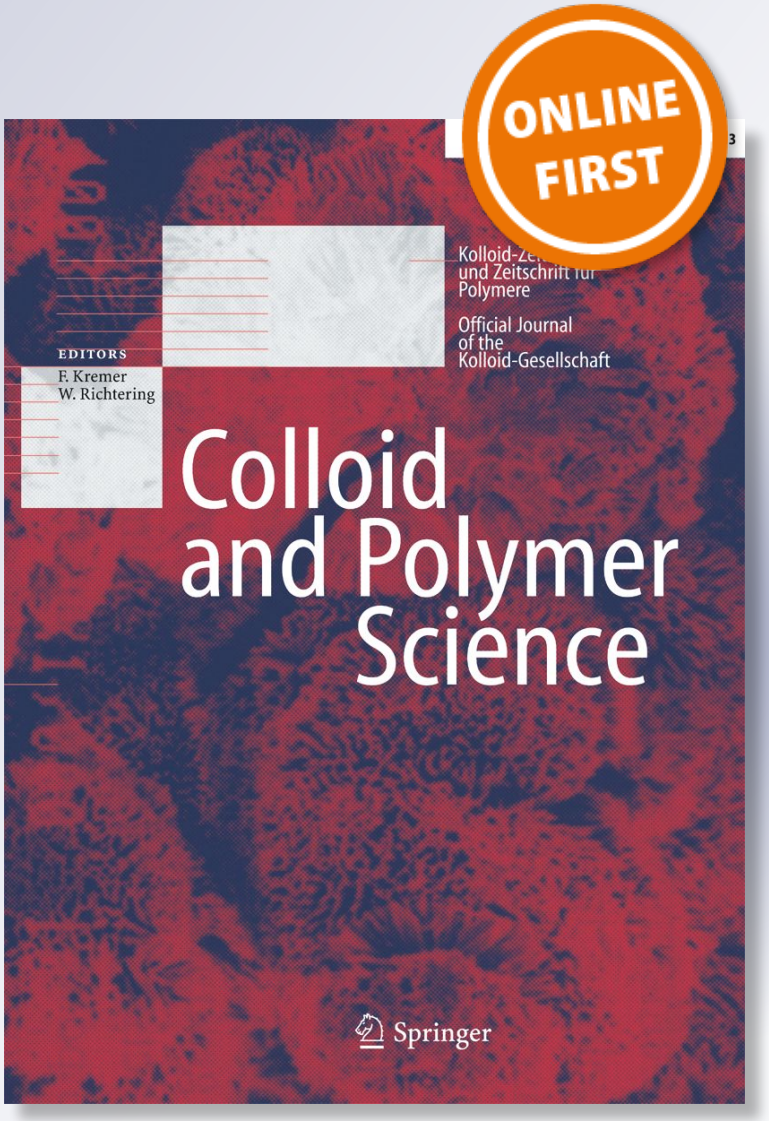

Springer

Colloid Polym Sci
DOI 10.1007/s00396-017-4190-x

ORIGINAL CONTRIBUTION

Assessment of synergistic interactions on self-assembled sodium alginate/nano-hydroxyapatite composites: to the conception of new bone tissue dressings

Luciano Benedini[1] · **Damián Placente**[1] · **Olga Pieroni**[1] · **Paula Messina**[1]

Received: 22 March 2017 / Revised: 3 July 2017 / Accepted: 24 August 2017

Abstract The aim of this work is to assess the behavior of biocomposites (CPSs) in regard to the generation of biogenic hydroxyapatite and also their degradation depending on the concentration of cross-linker agent, pH, and ionic strength. The development of these composites with potential application in bone tissue regeneration is based on alginate and synthetic nano-hydroxyapatite (nano-HA), which was used as a cross-linker agent. The CPSs showed the capability to develop biogenic hydroxyapatite when they were incubated in simulated body fluid (SBF) depending on the incubation time and concentration of the linker. These results were analyzed by x-ray diffraction (XRD), Fourier transform infrared (FT-IR), and scanning electron microscopy (SEM). Furthermore, the CPSs have shown resistance to the degradation (demonstrated by swelling and dissolution tests) when the mentioned conditions were modified. Finally, the development of a liquid crystalline phase within the composites, which contributes to reinforce their structure, is a novel finding in this study. This behavior has been shown by means of optical microscopy (OM) with crossed polaroids. Thus, these composites displayed promising results to be used as bone filling materials in the future.

Keywords Alginates · Nano-hydroxyapatite · Composites · Mesophases · Bone filling materials

Electronic supplementary material The online version of this article (https://doi.org/10.1007/s00396-017-4190-x) contains supplementary material, which is available to authorized users.

✉ Luciano Benedini
lbenedini@uns.edu.ar

[1] INQUISUR-CONICET, Department of Chemistry, Universidad Nacional del Sur, B8000CPB Bahía Blanca, Argentina

Introduction

Nowadays, autologous bone graft remains the gold standard for management of bone defects. However, there are some drawbacks associated with this methodology such as bone resorption, infections, limited availability of grafts, bleeding with further hematoma in the involved site, chronic pain with further increase in the donor-site morbidity, and also additional cost [1, 2]. Therefore, the design and development of new materials so as to replace the native bone in treatment of bone diseases are essential.

The materials used in tissue engineering must be biocompatible and act as a temporary 3D support for cell adhesion, deposition, and growth of the new extracellular matrix and also be able to be integrated into the surrounding tissue. Finally, the degradation of the devices must proceed in a controlled manner while maintaining their structural integrity until they are replaced by the new tissue [3]. In this context, ceramic materials were chosen for this application because of their good osteoconductive properties and osseointegration [4]. Ceramic materials for bone filling based on hydroxyapatite are used for treating bone deficiencies caused by illness state or injury [5]. The development of new bone is promoted by injection of this material into bone defects but replacing hydroxyapatite (HA) with host bone after implantation requires a long time nevertheless [6]. For this reason, the application of these ceramic materials requires the combination with other type of cements to strengthen their interaction between the bone cavity matrix and biomaterials and, thus, improve the adhesion of HA [7]. To overcome this issue, biocompatible biopolymers with bio-adhesion capability could be used. Within biopolymers, we can find alginates (ALGs), which are widely used for a variety of reasons such as their water-solubility, biodegradability, and thickening effect in certain conditions, with

Published online: 05 September 2017

capability of forming hydrogels in situ. As a consequence, composites based on alginate would be suitable to fill large bone defects and they would be easily absorbed by the patient's body. Furthermore, biogenic hydroxyapatite could be deposited when these biocomposites are incubated in simulated body fluid [8].

Some of the features required by alginates, which contribute to reach a suitable bone device, were previously described. However, there is another aspect that must be considered: the behavior of this polymer depends on pH values. This characteristic is important because the zone of the body affected by an injury displays a pH variation depending on naturally triggered biological processes [9]. Therefore, materials with pH adaptation capability could be considered for future designs of bone filling devices. Lin and Yeh [10] have reported that the presence of hydroxyapatite, along with alginate, increased the cell attachment in the inner parts of the bone matrix and offered a suitable choice of scaffold systems for bone tissue engineering. Hence, the developed composites might be applied in bone regeneration in combination with bioactive ceramics with promising results [11]. There is a strong interfacial interaction between alginate and hydroxyapatite by means of electrostatic forces and H bonds [11, 12]. However, the integrity of the composite is not kept by these forces alone. It has been reported that alginate and xanthan gum have helical structure and, under certain conditions, hydrogels formed by a blend of these two polymers [13, 14] can develop mesophases. From this perspective, our work is one of the first to report the development of these structures with alginate hydrogels. Furthermore, the mesophases could be used as drug delivery systems such as those reported by Quirolo et al. [15].

Therefore, biocomposites can keep their integrity in the tested media by means of the calcium effect, H bonds, electrostatic interactions, and liquid crystal formation. As a consequence, it has been reported that both the hydroxyapatite [16, 17] and alginate [18–20] can be used as carrier systems for one or more drugs [11, 21].

The aim of this work is to demonstrate that composites based on nano-HA (synthesized in our laboratory) and alginate can develop biogenic hydroxyapatite when they are incubated in SBF, and they have dissolution and swelling parameters that ensure their stability during the contact with body fluids and their conditions. These results were reached by comparing the effect of Ca^{2+} ions (provided by hydroxyapatite suspensions and, conversely, $CaCl_2$ solutions) on the hardness and strength of biocomposites and by assessing behavior when these structures are subjected to different solvents media which simulate the variability of pH in physiological conditions. Thus, this work tries to contribute with the understanding of biodegradable and bio-adhesive systems which could work as wound dressings potentially applicable to bone injuries or defects.

Materials and methods

Materials

Sodium alginate (ALG) with mannuronic/glucuronic acid ratio (M/G) estimated in 0.79 by ^{1}H NMR according to the literature [22] was purchased from Fluka (Switzerland, N: 71238, molecular weight (M_w) = 231,500 g mol^{-1}). Hexadecyl-trimethyl ammonium bromide (CTAB, M_w = 364.48 g mol^{-1}, 99% Sigma), a poly(propylene glycol) (PPG, Sigma-Aldrich, M_w = 425 g mol^{-1}, δ = 1.004 g cm^{-3} at 25 °C), sodium phosphate (Na_3PO_4, M_w = 148 g mol^{-1}, 96% Sigma), calcium chloride ($CaCl_2$, M_w = 91 g mol^{-1}, 99% Sigma), and sodium nitrite ($NaNO_2$, M_w = 69 g mol^{-1}, 97%) were used without further purification. For solution preparation, only triple-distilled water was used.

The nano-hydroxyapatite (nano-HA) was synthesized by means of micelles of CTAB with PPG. They form an organized hierarchical network which creates bioactive superstructures resulting in associations of nano-rods. Under synthesis conditions, CTAB forms rod-like micelles of 47 nm length that behaves as a template for deposition of PO_4^{-3} and Ca^{2+} ions. This procedure yielded a hydroxyapatite with the following formula: $Ca_{10}(PO_4)_6(OH)_2$ and with a M_w = 1004 g mol^{-1} [5]. The size and surface features of the nano-rods are very relevant for developing a good osseointegration. For this reason, PPG is used to reduce the size of the nano-rods and modify their topology for improving the cell adhesion [5].

Methods

Composite preparation

For this study, two types of biocomposites (CPSs) were developed with a water solution (W) (pH = 5.8) of alginate 2% (*w*/*v*). For the first type, synthetic nano-HA was used as cross-linking agent and, for the second one, $CaCl_2$ solution was utilized as a control set. Then, two other sets of CPSs were prepared using different solvents: (a) phosphate buffer saline (PBS) (pH = 7.4) and (b) acetate buffer (BAc) (pH = 4.2). The biocomposites prepared with (a) and (b) were developed to confirm the appearance of tridimensional ordered structures (mesophases) in the swelling tests, observed by means of optical microscopy (OM) in electronic supplementary material (ESM). The materials were labeled as Ca:CPSs and HA:CPSs depending on the kind of cross-linker agent used. The former composites were prepared using external cross-linking, by adding $CaCl_2$ in three different concentrations, whereas the latter were developed utilizing three different concentrations of previously synthesized nano-HA as the cross-linking agent. Finally, the last group of CPSs was obtained using both $CaCl_2$ and nano-HA (Ca1/HA2:CPS). In this final set, the used concentrations were Ca1 and HA2 for $CaCl_2$ and nano-HA,

respectively. The procedure is described as follows: 15 ml of alginate solutions (in water, phosphate buffer or acetate) were put into petri dishes and different amounts of cross-linking agents containing solutions were added. For this purpose, the concentrations used to cross-link the CPSs were in accordance with the molar mass of the reagents ($CaCl_2$ and HA). The biocomposites labeled Ca1 were developed by adding 1 ml of a 110 mM $CaCl_2$ solution to 15 ml of 2% (*w*/*v*) alginate solution. For Ca2 and Ca3, 2 and 3 ml of 110 mM $CaCl_2$ were added, respectively. The composites called HA:CPS were developed by adding 1, 2, and 3 ml of a 11 mM of HA suspension to 15 ml of 2% alginate solution (*w*/*v*), and they were consequently called HA1:CPS, HA2:CPS, and HA3:CPS. Thus, the amount of calcium in Ca:CPSs was the same as in HA:CPSs. Once prepared, the CPSs were dried up to constant weight at 60 °C during 24 h in an electric oven. Then, they were rehydrated with their respective solution (water, PBS, or BAc) and dried to reach a more homogenous point consistency.

At the same time, biocomposites with a solution of alginate 1% (*w*/*v*) and Ca2 of $CaCl_2$ and HA2 of nano-HA concentrations as cross-linking agents were studied in the three mentioned media (water, and phosphate and acetate buffers). However, since these dissolve in a short time, we only observed them by OM (shown in ESM) as any other study would have been unproductive.

Swelling ratio test

Swelling ratio test of biocomposites was used as a measure of the extent of cross-linking or, in other words, as a measure of the effect of cross-linking agents depending on the different media. Previously weighted, they were incubated at 37 °C in different solvents during 10, 60, and 1440 min. The used solvents were as follows: water (W) (pH = 5.8), acetate buffer (BAc) (pH = 4.2), and phosphate-buffered saline (PBS) (pH = 7.4).

Once swollen in these different solvents, the biocomposites were weighed again. Finally, a relation between final weight (W_f) and initial weight (W_i) was established following the Rhim method [23]:

$$\mathrm{SW} = \frac{W\mathrm{f}}{W\mathrm{i}} \times 100 \tag{1}$$

Measurements were done three times on independent experiments and the results are shown in the ESM as mean values of the three assayed replicates ± the standard deviation.

Dissolution test

The dissolution assay has been performed to evaluate the degree in which the biocomposites keep their mass and consistency after incubation at 37 °C during 10, 60, and 1440 min. In addition, the difference in their behavior at different pH values could be evaluated. The dried biocomposites were weighted and then incubated in water, acetate buffer, or phosphate-buffered solution during the mentioned time. Finally, they were removed from the incubation solutions and dried up in the oven up to constant weight. Thus, relations between final (W_f) and initial (W_i) dried weights were established as follows:

$$\mathrm{DT} = \frac{(W\mathrm{i} - W\mathrm{f})}{W\mathrm{i}} \times 100 \tag{2}$$

Measurements were done three times on independent experiments and the results were shown as mean values of the three assayed replicates ± the standard deviation.

Optical microscopy

Optical microscope micropictures were carried out with a Nikon Eclipse E-200 POL polarizing microscope (Tokyo, Japan). All samples were laid on excavated slides and dried up to constant weight in the oven at 60 °C during approximately 1 h. This exposition time is shorter than those presented in the "Composite preparation" section because of the smaller thickness of the structures. Microphotographs were taken with and without crossed polarizers, and in some cases, a 1λ retardation plate was intercalated.

Bioactivity assay

To carry out the bioactivity assay, the material was kept in contact with simulated body fluid (SBF) following the standard procedure described by Kokubo et al. [8, 24, 25], which has a composition and ionic concentration similar to those of human plasma, containing Na^+ (142.0 mM), 211 K^+ (5.0 mM), Mg^{2+} (1.5 mM), Ca^{2+} (2.5 mM), Cl^- (148.8 mM), HCO_3^- (4.2 mM), HPO4^{-2} (1.0 mM), and SO_4^{-2} (0.5 mM). The synthesized materials were immersed in 1.5 SBF at 37 °C for periods of 7, 15, and 30 days; the specimens were removed from fluid, rinsed with distilled water, and finally dried. The temperature (37 °C) was maintained by placing the samples in a thermostatic bath throughout the experiment.

FT-IR spectroscopy The FT-IR spectra were obtained in 4000–400 cm^{-1} wavelength range by a NICOLET Nexus 470 spectrophotometer, with a 2-cm^{-1} resolution and 64 scans/min using an AVATAR Smart Diffuse Reflectance Accessory.

The samples were performed at 1% weight/weight in KBr; therefore, 2 mg of either oven-dried sample and 200 mg of

KBr (FT-IR grade, Aldrich Chemical Co.) were homogenized thoroughly in an agate mortar with precaution taken to avoid the moisture.

After grinding, the sample mixture was heaped over the top of the microsample cup. Any excess material was removed with a straight edged tool. For the background, a microsample cup of pure KBr was prepared. Each record was done in triplicate.

Scanning electron microscopy The SEM micropictures were obtained using a JEOL 35CF, Tokyo, Japan. The composites treated as described in the "FT-IR spectroscopy" section were observed using a SEM to explore the surface morphology and evaluate their changes.

X-ray powder diffraction Powder X-ray diffraction (XRD) data were collected with a Philips PW 1710 diffractometer with Cu Kα radiation (λ = 1.5418 nm) and graphite monochromator, operated at 45 kV, 30 mA, and 25 °C. The mean crystalline size (δ) of the particles was calculated from XRD line broadening measurement using the Scherrer equation [5, 26]:

$$\delta = \frac{0.89\lambda}{\beta\cos\theta} \tag{3}$$

where λ is the wavelength (Cu Kα), β is the full width at the half maximum of the hydroxyapatite (211) line, and θ is the diffraction angle. The fraction of crystalline phase (Xc) of these ceramics was evaluated by the following equation [5, 26]:

$$\mathrm{Xc} = \frac{1-\upsilon_{112/300}}{I_{300}} \tag{4}$$

where I_{300} is the intensity of (300) diffraction peak and $I_{112/300}$ the intensity of the hollow between (112) and (300) hydroxyapatite diffraction peaks. The estimated uncertainties are about 20% [5].

All the biocomposites were dried in an oven after the incubation time and then washed with distilled water and dried again. This protocol was repeated twice and finally XRD measurements were carried out. It is important to remark that XRD measurements were performed before and after the incubation process to establish a ratio between hydroxyapatite used as a linker and the biogenic hydroxyapatite produced during the incubation. This procedure was performed with three independent samples and therefore biocomposites with same (dried) weights were used for the comparison.

Results and discussion

Relation between features of the biocomposites and the formation of biogenic hydroxyapatite

The fact that each polymer has its own influence on the nucleation and growth of hydroxyapatite nanocrystals by specific organic–inorganic interactions between components [27] highlights the importance of the polymer election. Kokubo et al. [8] have shown that bone-like apatite can deposited onto organic polymer gels surfaces containing carboxylic groups after their incubation in simulated body fluid. In the current work, this behavior was demonstrated by FT-IR, SEM, and XRD.

The FT-IR spectra of HA2:CPSs are shown in Fig. 1a. The three spectra correspond to different incubation times (black solid line, 7 incubation days; black dashed line, 15 days; and dark gray solid line, 30 days). In this figure, three important bands named A, B, and C are displayed. A and B bands at 1613 and 1400 cm^{-1} correspond to asymmetric and symmetric stretching of vibration bands of carboxylates (COO^-) groups, respectively. The presence of these bands indicates that biocomposites have a certain number of free COO^- groups working as nucleation sites, from which the growing of biogenic hydroxyapatite is generated. In this spectrum, the

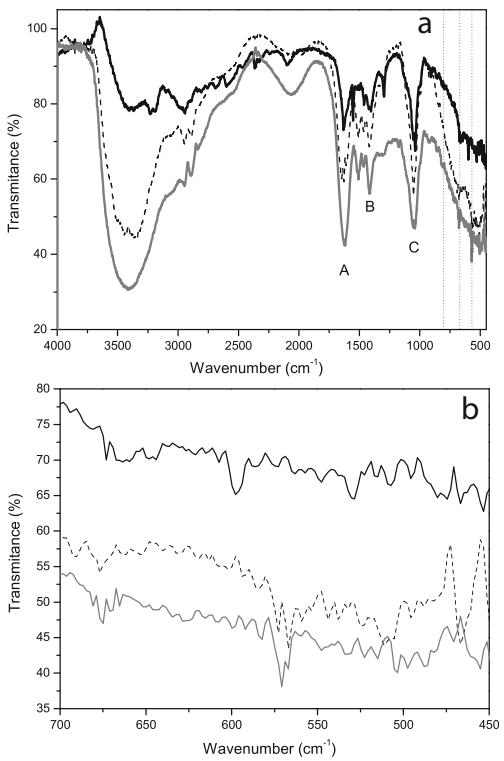

Fig. 1 **a** FT-IR of biocomposites with concentration 2 of nano-HA as a cross-linker and incubated in SBF. Black solid line, 7 incubation days; black dashed line, 15 days; and dark gray solid line, 30 days. **b** Magnification of **a** between 700 and 450 cm^{-1}

C band at 1098 cm^{-1} corresponds to phosphate (PO_4^{3-}) group of hydroxyapatite [28, 29]. Additionally, it demonstrates that an increase in incubation time generates an increase in the hydoxyapatite growth. Despite this, there was no considerable difference between biocomposites with incubation times of 15 and 30 days. A greater splitting of this band (C) indicates higher crystallinity of the hydoxyapatite. There are other bands in this figure that indicate its presence, and therefore, they are represented with dotted lines and correspond to the following bands: 560–600 cm^{-1} (which represents the vibration band of phosphate (PO_4^{3-}) group) and 670 cm^{-1} (which represents the carbonate hydroxyapatite (CO_3:HA) formation). It has been assumed that all the bands ascribed to PO_4^{3-} group correspond to the hydroxyapatite because of the results obtained by XRD which are discussed below (see Fig. 4).

For better comprehension, a magnification of the zone between 450 and 700 cm^{-1} is displayed in Fig. 1b. Hence, when nano-hydroxyapatite is used as cross-linker, the band of carbonate group of carbonate hydroxyapatite appears (at 670 cm^{-1}) independently of the incubation time (7, 15, or 30 days) in simulated body fluid. It is clearly noted that, an increase of the peak at 560–600 cm^{-1} represents the presence of biogenic hydroxyapatite in the system when incubated during 15 days or more. Finally, the vibration modes between calcium ions and carboxylate groups of alginate at 819 cm^{-1} are shown. From the analysis of the region between 3000 and 3700 cm^{-1}, almost five peaks can be recognized related to the oxygen and hydrogen stretching. The band at 3440 cm^{-1} corresponds to adsorbed water and the others, located at 3744, 3223, 3100, and 3000 cm^{-1}, may be assigned to different structural OH groups in hydroxyapatite crystals [5] (–OH groups associated to phosphate groups, and others with minor interactions with the environment).

Therefore, for all the biocomposites performed and incubated during 15 days into SBF, the FT-IR spectra displays an important increase in the band at 1036 cm^{-1} corresponding to the (v_3) phosphate (PO_4^{3-}) absorption which is associated to the growth of hydroxyapatite coating on their surface. These results agree with those reported by Ruso et al. [30]. Biocomposites cross-linked with nano-hydoxyapatite showed a clearly superior (v_3) PO_4^{3-} adsorption band intensity when compared to those which use $CaCl_2$ as cross-linker, and this effect was confirmed by scanning electron microscopy (SEM) (see Fig. 3). This behavior is associated to the material's bioactivity and its osseointegration capacity and is in agreement with the work of Kokubo et al. [8]. It is important to remark that the HA:CPSs with 7 days of incubation did not show neither the peak presence at 560–600 cm^{-1} nor an increase in the peak at 1036 cm^{-1} corresponding to the (v_3) phosphate (PO_4^{3-}) absorption; therefore, the biogenic capability of the biocomposites into simulated body fluid is clearly noted after 15 days of incubation. However, this last peak at 1036 cm^{-1} appeared when synthesized hydroxyapatite was used as a cross-linker. Furthermore, the obtained results confirm an increase in the CPSs' bioactivity by the incorporation of nano-HA.

Figure 2a shows the complete FT-IR spectra of biocomposites prepared in water incubated in SBF during 15 days. Figure 2b shows a magnification of these spectra between 700 and 450 cm^{-1}. Here, the vibration band of phosphate (PO_4^{3-}) group of hydroxyapatite 560–600 cm^{-1} is more evident for HA:CPSs than for Ca:CPSs. However, for Ca2:CPS, this peak is also evident. This band confirms that these biocomposites can develop biogenic hydroxyapatite

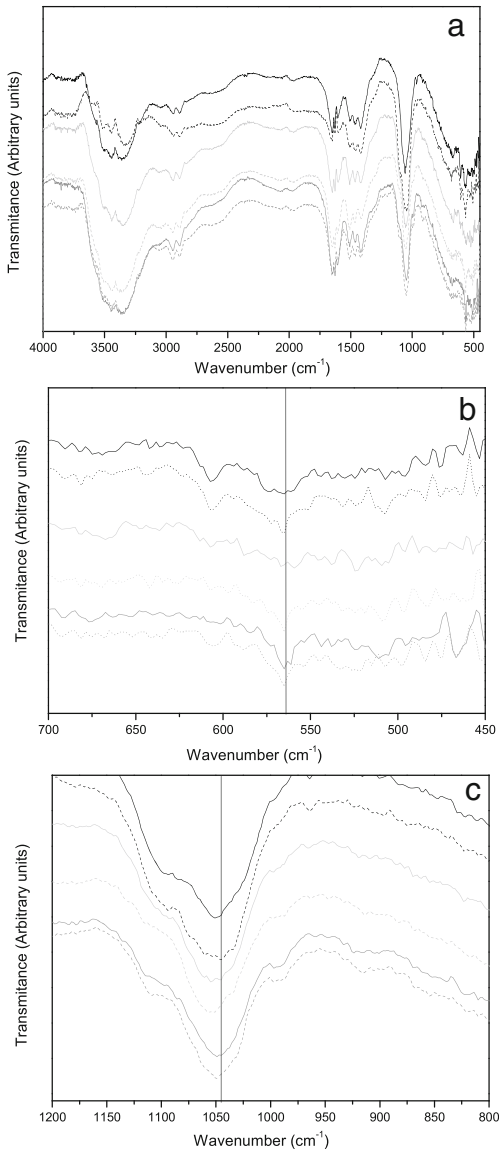

Fig. 2 **a** FT-IR of ALG 2% *w/v* biocomposites incubated in SBF 15 days. Three of them use $CaCl_2$ as a cross-linker and other three use nano-HA. Black solid line, Ca1; black dashed line, Ca2; light gray solid line, Ca3; light gray solid line, HA1; dark gray solid line, HA2; and dark gray solid line, HA3. **b** Magnification of **a** between 700 and 450 cm^{-1}. **c** Magnification of **a** between 1200 and 800 cm^{-1}

when are incubated in SBF during 15 days. Figure 2c shows a magnification of the spectra between 1200 and 800 cm^{-1}. As mentioned above, the band at 1036 cm^{-1} corresponds to the (v_3) PO_4^{3-} absorption band and is associated to the growth of an HA coating on their surface. Based on this study, we can affirm that our system generates a coating of biogenic hydroxyapatite in SBF after 15 days of incubation.

Figure 3 shows SEM micropictures of biocomposites developed in water and incubated in SBF. Figure 3a, b corresponds to composites with concentration 2 of nano-HA, with an incubation time of 7 and 15 days, respectively. Crystals with sizes between 0.5 and 2 μm are shown. Similar results with bigger crystals sizes were reported by Zhang [31]. In these figures, it is possible to see that an increase of incubation time generates larger cumulous of biogenic hydroxyapatite, always with the same features. Figure 3c shows a CPS cross-linked with $CaCl_2$ (Ca2) with 15 days of incubation. Here, the cumulous of biogenic hydroxyapatite is smaller than the one presented in Fig. 3a, b (HA:CPS) and detectable by FT-IR. Figure 3d shows a 30-day incubated CPS cross-linked with HA2 concentration. It is possible to note that biogenic hydroxyapatite is growing inside the biocomposites with features similar to the ones observed in other assays.

Therefore, these pictures show that an increase of incubation time of our materials into SBF generates more biogenic hydroxyapatite and that the growth increases when using nano-HA as a cross-linker instead of $CaCl_2$.

Figure 4 shows the X-ray diffraction patterns of three biocomposites built in water and then incubated during 15 days in SBF. The composites were carried out using concentration 2 of nano-HA (dark gray), concentration 2 of $CaCl_2$ (light gray), and concentrations 2 and 1 of both nano-HA and $CaCl_2$ (black line) as cross-linkers, respectively. All the observed peaks are readily indexed and are in agreement with those reported by D'Elía et al. [5]. The patterns presented in this figure reinforce the fact that our materials cross-linked with nano-HA generate more biogenic hydroxyapatite than those with $CaCl_2$.

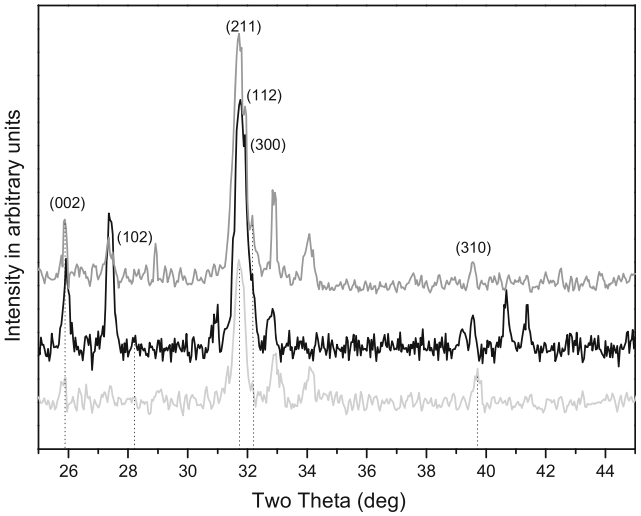

Fig. 4 XRD of biocomposites incubated in SBF during 15 days. Solid black line, HA2 + Ca1; light gray line, Ca2; dark gray line, HA2

Accordingly, biogenic hydroxyapatite can grow on the surface of composites, depending mainly on the chosen polymer (which has negative charged groups), the presence of synthesized hydroxyapatite used as cross-linker, and the incubation time.

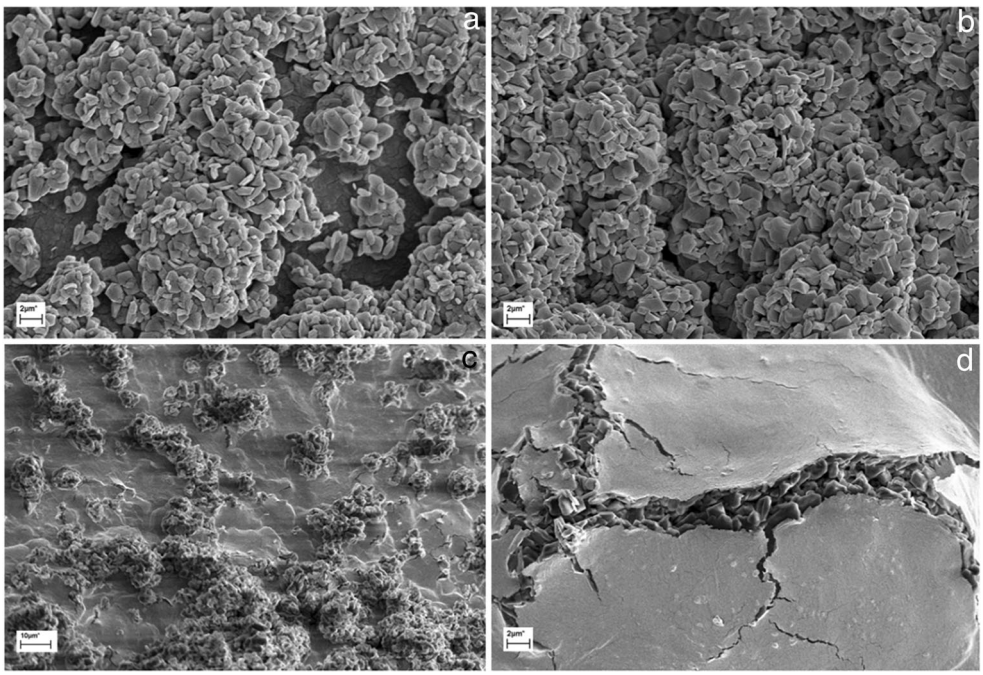

Fig. 3 SEM images of biocomposites developed in water (with and without HA) and incubated in SBF: **a** 7 incubation days, HA2; **b** 15 incubation days, HA2; **c** 15 incubation days, Ca2; **d** 30 incubation days, HA2

Effect of concentration of nano-HA, pH, and ionic strength in the stability of the biocomposites (CPSs)

The pH and ionic strength have a great implication on the stability of biocomposites. The assessment of the stability was carried out by means of swelling tests and dissolution tests. Optical microscopy (OM) was used to confirm the liquid crystals formation inside the materials.

The swelling and dissolution studies were carried out in three different media at 37 °C: phosphate buffered saline (PBS) (pH = 7.4), water (pH = 6), and acetate buffer (pH = 4.2). PBS was chosen because the physiological pH is approximately 7.4. Likewise, water and acetate buffer were chosen because their pH is similar to the cellular interaction pH and by-osteoblast remodeling pH, respectively [9].

The first group of nano-HA composites (HA:CPSs) was developed in water and incubated in water. The dissolution test results are shown in Table 1 (electronic supplementary material, ESM). All the HA:CPSs show that their mass decreases when the incubation time increases, reaching a complete loss of composites mass at 1440 min.

A swelling ratio test was conducted using three biocomposites with different nano-HA concentrations, varying from HA1 to HA3. No significant differences were observed after 10 min of immersion. However, the recovered mass of HA2 and HA3 CPSs was almost twice the recovered mass of HA1:CPS after 60 min. The control group (Ca1, Ca2, and Ca3:CPSs) shows a typical behavior for these kinds of systems: the swelling ratio test values increase as the incubation time increases. In addition, an increase of the cross-linker concentration decreases the swelling values as was reported by Rhim et al. [23]. This effect could be explained by the fact that the increase of the cross-linking agent quantity decreases the capability of biocomposites to absorb water because of the closeness among alginate chains. Nevertheless, this factor becomes less relevant as the media exposure time increases.

The effect of phosphate-buffered saline (pH = 7.4) in swelling test values for biocomposites developed in water is shown in Table 2 of electronic supplementary material, ESM. Here, the swelling values for the different composites did not change after 60 min of incubation. However, unlike biocomposites incubated in water, these did not reach their complete dissolution after 1440 min of incubation. By comparing Ca:CPSs submerged in water with those immersed in phosphate buffer, it is shown that they are similar terms of value but not so in terms of their exterior aspect, as the latter are slimier and stickier. This could be explained by the presence of carboxylate groups on the backbone of alginate chains which confers a pH-dependent stability. The response to pH variation is evident from higher swelling ratios reached with bigger pH values (to compare Table 2 with Table 3 ESM) due to chain expansion from the presence of ionized carboxylate groups on the backbone. For this reason, swelling ratios in phosphate-buffered saline are higher than in other solvents.

Table 3 ESM shows the results of swelling test in acetate buffer. This assay and the previous one (in phosphate solution) show the role of pH in the behavior of biocomposites. For each measured time (10, 60, and 1440 min), the swelling test values for HA:CPSs were higher than those for Ca:CPSs; but inside each group, no changes were evidenced with the increase of incubation time and the concentrations of nano-HA and $CaCl_2$. This finding suggests that a resistant structure is formed from nano-HA's calcium dissolution, which generates new cross-linking points that improve the biocomposites' strength. Therefore, HA:CPSs soaked in acetate buffer show a bigger change in their behavior depending on pH conditions than those soaked into phosphate buffer and, consequently, could be potentially used to develop drug delivery systems such as those reported by Lucinda-Silva et al. [29]. In this contribution, the researchers were able to achieve faster drug releases based on systems with high swelling degrees. In consequence, the design of a pH-dependent drug delivery system is proposed as future work.

In addition to the release of ions, produced by the change of pH, there are other structures that also contribute with the reinforcement of reticulation of composites. For this reason, the emergence of ordered structures (liquid crystals) helps to maintain the structure of composites as by optical microscopy (Fig. 6). Therefore, finding these structures (which are more visible in the case of acetate buffer) supports the fact that the biocomposites did not dissolve during our experiments using the mentioned media. One of the advantages of using nano-HA as the cross-linking agent is that the composites developed resistant structures at cellular interaction pH, without the need to use high concentrations of $CaCl_2$ (which increases their hardness) and, therefore, obtaining very versatile materials. However, to keep this versatility, strength, and capability of developing these ordered structures at all employed pHs, a small amount of $CaCl_2$ is need. In addition, $CaCl_2$ is needed to keep the integrity of composites at pH = 6. Table 4 ESM displays the swelling test of the materials made with HA2 and Ca1 concentrations, which were incubated in different media. The assay shows that biocomposites did not dissolve completely despite the media they were submerged into. Therefore, the use of small amounts of $CaCl_2$ is necessary to guarantee the stability of the biocomposites at any human body pH value.

The main in vivo degradation mechanism of alginate-based biomaterials is the disintegration of the material due to the gradual exchange of calcium ions with sodium ones. The alginate (ALG) chains themselves are relatively stable under physiological conditions (pH = 7.4 at 37 °C) and are susceptible to degradation by reactive oxygen species [32]. However, its optimum stability is reached at pH = 6. Usually, it is necessary to use calcium salts ($CaCl_2$ and $CaCO_3$) or divalent/

trivalent cations (as cross-linking agents) for gelation and ALG resistance improvement [33]. Magnesium ions in high concentrations can be used [34]. This gelation mechanism is known as external gelation and is extremely safe for cells; it has been widely used in medicine, including cell therapy and tissue engineering [35]. If calcium ions are used, these are released from the matrix by reducing the pH, which increases its degradability [36]. Other kind of external gelation is also produced by other sources of calcium (e.g., calcium precipitates) where the ion interacts with the exterior surface shell of the polymer droplet such as in the foam of alginate. Other type of formation of beads is produced by means of water-in-oil emulsions where the calcium is dispersed in the organic phase. There is also another mechanism known as internal gelation, which is produced by the inclusion of D-gluconic δ acid lactone (GDL) in an alginate solution where hydroxyapatite is added [37]. This gelation is triggered in situ by the instantaneous release of calcium (from an insoluble salt) via gentle pH adjustment as reported by Pinto Reis et al. [38]. This process generates more homogeneous matrices by means of a slow release of calcium ions through insoluble salts when exposed to low pH values [39]. However, the pH value for internal gelation must be controlled owing to the rate of acid hydrolysis for alginates at pH around 3 or 4 being higher than those for neutral polysaccharides [40]. For this reason, the gelling kinetics is strongly dependent on the method used for the introduction of the cross-linking ions, and hence, homogeneous or inhomogeneous hydrogel can be obtained. Due to that fact, composites based on alginate can reach a stable state at low pH, keeping their partial structure and furthermore, guaranteeing that the system could interact with the damaged tissue during the need time. Since this polymer is an acidic polyelectrolyte, it is important to note that the p*K*a value, as well as the enthalpy of dissociation, depends on the degree of dissociation and, therefore, on the solutions' pH value used for preparing the hydrogels which is relevant to perform these hybrid systems.

Biocomposites prepared only with nano-HA have enough biogenic activity (see the "Bioactivity assay" section) but more resistance is needed to behave as an effective bone tissue dressing. For this reason, we carry out a study using the first concentration of $CaCl_2$ (Ca1) and the second concentration of nano-HA (HA2) as cross-linkers to keep the biogenic activity and improve their resistance. In this work, a part of nano-HA is dissolved by decreasing the pH values, thus providing calcium ions which can improve the resistance of the composites. Therefore, a decrease of pH values will not lead to the degradation of the composites unlike the behavior previously observed in traditional gels. Hence, a pH decrease (such as the one produced by cell remodeling states) will not produce an early degradation of these materials.

The dissolution test, just like the swelling study, was performed using three different media: water (pH = 5.9), phosphate-buffered saline (PBS) (pH = 7.4), and acetate buffer (pH = 4.2).

Table 5 ESM shows the dissolution test values in water, represented as the percentage of dissolved mass of HA:CPSs and control CPSs (Ca:CPSs = Ca1, Ca2, and Ca3). In this table, no significant differences among the HA:CPSs are shown when the amount of nano-HA in the composites is increased. The Ca:CPSs' dissolved mass increases with longer incubation times, as well as with the decrease of the concentration of calcium ions in the aforementioned composites. The biocomposites tested in phosphate buffer are shown in Table 6 ESM. Here, contrary to what happened with those incubated in water, the increase of incubation time and nano-HA concentration did not change the dissolution values between 60 and 1440 min., and therefore, the composites did not reach their complete dissolution after 1440. This probably occurs due to the formation of ordered structures such as the mesophases shown in Fig. 5b. Table 7 ESM shows the dissolution values of biocomposites into acetate buffer. Here, no significant differences are evidenced among the three HA:CPSs. This is likely due to the formation of mesophases, which reinforce the structure, and because of the release of calcium ions from nano-HA (used as a cross-linker) when pH value is reduced. The liquid crystal phases are shown in Fig. 5c. The formation of these phases supports the results displayed in Table 8 ESM, where HA:CPSs dissolution is reduced by the calcium ions provided by $CaCl_2$. The FT-IRs show a decrease in the band between 600 and 550 cm^{-1} which confirms that the nano-HA, used as a cross-linker at low pH, dissolves when exposed to physiological medium. The internal gelation is presumably what reinforces the alginate chains.

Figure 5 shows biocomposites developed in water, which change their structure depending the media in which were soaked. The pictures displayed were obtained using an optical microscope with a retardation plate. The biocomposites developed in water with HA2 concentration and immersed in acetate buffer solution formed a liquid crystal phase. Figure 5a shows this behavior, which had not been reported in the consulted literature. Figure 5b shows the PBS-submerged composites and their birrefringent structures. Finally, Fig. 5c clearly shows the formation of a liquid crystal phase in the materials cross-linked with both HA2 and Ca1 and soaked in acetate buffer solution.

It is important to note that the biocomposites that were submerged into buffer solutions display birrefringent structures and those immersed in water do not. Particularly, the materials immersed in acetate buffer developed more ordered structures. This behavior has been reported by Williams and Phillips [41] for different mixtures made with alginate and xanthan gum, which form ordered phases in a wide range of concentrations [42]. Other mesophase was characterized as pre-cholestecic when cellulose nanocrystals were included in alginate gels and also with inorganic materials such as silica

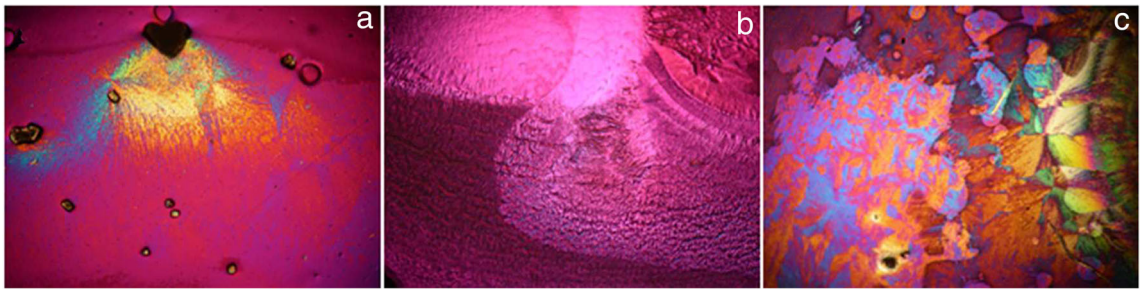

Fig. 5 Micropictures of biocomposites of ALG 2% *w/v* performed in water and then dissolved in solvents and returned to dry. **a** CPS with HA dissolved with BAc. **b** CPS with HA dissolved with PBS. **c** CPS with HA2 + Ca1 dissolved with BAc

[43]. This behavior is possible because macromolecules such as this polymer can develop ordered structures under certain conditions (concentration, temperature, and ionic strength) [44]. These structures also appear with lower concentrations of ALG (see Figures 1 and 2 of the ESM).

The influence of the solvents in the biocomposites demonstrated that different structures are generated. With these tests, it is possible to show that they have a pH-dependent behavior. For this reason, their use as a filling material shows promising results when these materials are subject to the different pH ranges at physiological conditions. Other findings have revealed that an order-disorder transition of aqueous xanthan gum/acacia gum blends depends on the pH values, the ionic strength, and the ion exchange, which affect the stability and helical conformation of xanthan gum molecules [45].

Our samples are too coarse to display simple textures as oil streaks or spherulites; however, interference colors are really notorious. Owing to the helical and rod-like structure of xanthan gum and a very large number of inter- and intramolecular associations, several liquid crystalline characteristics have been reported [13, 14]. Therefore, in a polyelectrolyte, the distance between two charged groups depends on the spatial conformation. When polymers adopt helical conformation, this structure is stabilized by a decrease of the temperature or increase of the external salt concentration. Therefore, large rod chains form and stay in their spatial position, thus developing stable mesophases. For this reason, the liquid crystal phases appear with the increase of salt and no birrefringent phases are shown when water is used as soak medium. Thus, biocomposites developed in water and then soaked with different saline solutions (which simulate the physiological conditions) can develop liquid crystal phases.

The FT-IR spectra of biocomposites developed with both $CaCl_2$ and nano-HA as cross-linkers and acetate buffer (see the "Composite preparation" section) are shown in Fig. 6. It is important to remark that these composites prepared using acetate buffer as a solvent with or without nano-HA did not present the peaks between 600 and 550 cm^{-1} after incubation in SBF. This finding confirms that the nano-HA used as a cross-linker in these composites and then exposed to physiological medium is dissolved by means of internal gelation and, due to this fact, the provided Ca^{2+} ions from nano-HA conserve the structure of the biocomposites during more time. For this reason, these materials present lower dissolution rates and lower swelling ratios. After the reinforcement of their structure, there are more bridges formed between Ca^{2+} ions and carboxylic groups of alginate chains, and, as a consequence,

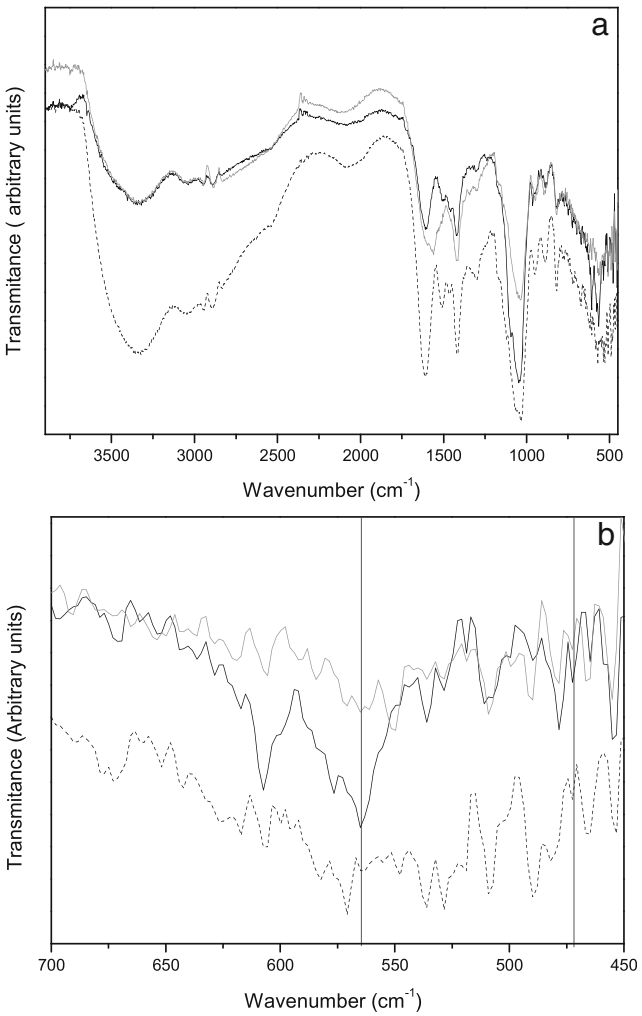

Fig. 6 **a** Biocomposites using $CaCl_2$ and HA as cross-linkers (Ca1HA2) and kept incubated 15 days in SBF: black solid, the materials developed in water. Dashed black line in PBS and dark gray line in BAc. **b** Magnification of **a** between 700 and 450 cm^{-1}

these negatively charged carboxylic groups will not be available for the deposit of biogenic hydroxyapatite.

Influence of the ionic strength of media in the liquid crystal formation and composites aspect

The electrostatic interactions strongly modify the properties in polyelectrolytic polymers solutions, due to the screening effects when salts are added. These effects are characterized by Debye length that establishes the distance in which electrostatic charges are screened [46]. Owing to that fact, an increase in ionic strength generates not only an order between the alginate chains but also keeps their fluidity. This behavior, associated with those generated by pH modifications, enables the occurrence of liquid crystal phases. Therefore, the formation of anisotropic phases is associated with the well-oriented 2D structure of polymer chains depending on their ionization state which is conditioned by pH, the screening role of the ions of the solution (ionic strength), and also the Ca^{2+} presence which reinforce the ordering of the gel. The atomistic structure of the junction zone of alginate gels is commonly described in the light of the "egg-box" model initially proposed by Grant et al. [47]. Therefore, chains associate in a regular helical conformation providing specific sites for the chelation of calcium ions via tight binding interaction with two carboxylate groups and a number of sugar hydroxyl groups from the two chains [48].

Alginate is composed by a linear hetero-polysaccharide formed of two different monomers (1 → 4)-β-linked: the β-D-mannuronic acid (M) and the α-L-glucuronic acid (G). The presence of carboxylic groups makes it behave as an anionic substance, exhibiting a pH responsive behavior, and thus, it presents higher swelling ratios when pH values are increased because the carboxyl groups of both mannuronic acid (p*K*a = 3.38) and glucuronic acid (p*K*a = 3.65) are ionized. Therefore, if the pH of the ALG-containing solution is lowered below the p*K*a of the constituting acids, phase separation or hydrogel formation occurs. Several investigations have focused on the pH dependence of alginic acid precipitation. It was found that molecular weight and composition play an important role in determining the pH of the precipitation of the polysaccharide [40]. In particular, MG-block-rich alginate show a reduced tendency to phase-separate at acidic pH values when compared with G- and M-rich alginates, likely because of their higher degree of "conformational disorder" of the glycosidic bonds [49]. Ionically cross-linked alginate hydrogel disperses via an ion exchange process involving loss of divalent ions into the surrounding medium. However, the speed of gelation is too fast to be controlled due to the high solubility of calcium chloride in aqueous solution, and for this reason, it is mandatory to dry and then re-hydrate the materials to reach a homogenous texture. The lack of composites homogeneity limits their application on injectable scaffolds. Therefore, the gelation speed affects the gel uniformity and strength directly. In order to slow and control the gelation, $CaCl_2$ can be replaced by calcium sulfate ($CaSO_4$) or calcium carbonates ($CaCO_3$) which have lower solubility. In this study, $CaCl_2$ is replaced by nano-HA and the composites made with calcium chloride are used as control.

A probable behavior is shown in Fig. 7. This behavior could be developed into living systems and is schematized as follows: in physiological conditions of pH (pH = 7.4) and ionic strength, the shapes of these compounds developed with water as solvent could be distorted, but part of it is maintained by the arisen of mesophases perceived as birefringence zones by optical microscopy (less birefringence than in acetate buffer). This condition would, on the one hand, favor the release a part of an active substance potentially contained into the matrix and, on the other hand, enable the infiltration of cells responsible for bone remodeling that would cause a decrease in pH values (to 4.2) inside of the materials. This decrease of pH would generate an increase of their resistance through the release of Ca^{2+} ions from nano-HA (corroborated in swelling and dissolution tests) and the arising of a birrefringent structure of liquid crystal which help the structuration of biocomposites. In this context, our systems would acquire an additional resistance by the reinforcement of the liquid crystal matrix (corroborated by optical microscopy) that could cause the reduction of the release of active ingredients. On the other hand, the growth of biogenic hydroxyapatite, which is promoted by the remainder of the nano-HA synthetic included in the composites, is evidenced onto and inside the matrix (see SEM micropictures). This manifests when materials are incubated in SBF irrespective of whether they are subjected to

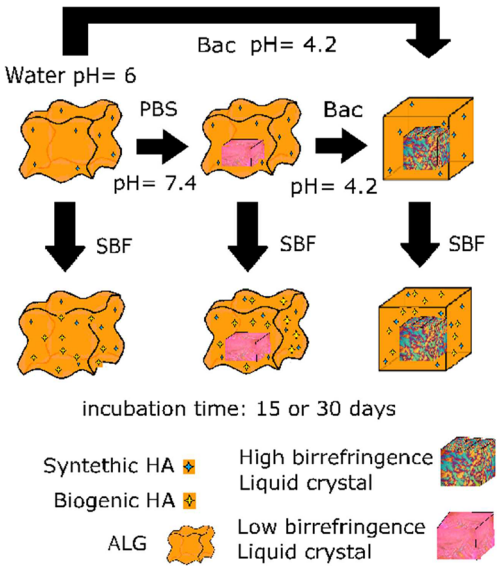

Fig. 7 Biocomposites in different media and then incubated in SBF. The orange cube represents the composites and the colored cube inside them represents the liquid crystal formation which appears with the modification of ionic strength. Light blue stars represent synthetic hydroxyapatite and the yellow ones, the biogenic

solutions with different pH and ionic strength (acetate or phosphate buffers).

Drug delivery by organized systems

Hydrophilic matrix systems have become relevant because they can be applied to sustained-release drug delivery systems, as a result of their excellent uniformity and ease of manufacture. There are many examples which describe the capability of the gels to carry out these systems and also others when they are combined with ceramics materials [16, 18, 19, 50, 51]. In addition, the development of liquid crystal phases improves the use prospects of biocomposites owing to their potential utilization as drug delivery systems. The use in drug delivery is possible because liquid crystals can retain a drug inside of their lattice and then this active substance can be released from this 3D structure by a disassembly process which loses its shape [15]. In this context, there are different systems that report the use of liquid crystals for drug delivery such as those proposed to deliver antioxidants and vaccine co-adjuvants [52, 53]. Accordingly, we propose three different mechanisms by which our composites could carry a drug: the first, by adsorption of the drug onto nano-HA; the second, retained among alginate chains by interaction of electrostatic forces between the charged groups and ions; and finally, by means of interaction with the liquid crystal matrix.

Conclusion

The relevance of this work lies on the assessment of biocomposites developed between with nano-hydroxyapatite synthesized in our laboratory, with proven osteoconduction and osseointegration capabilities, and a bio-adhesive biocompatible polymer such as alginate. One of the most important findings of this work is that composites could serve as filler material in bone diseases. Other important accomplishment is that their stability at low pH values has considerably been improved. It was shown that the biocomposites develop biogenic hydroxyapatite when incubated in simulated body fluid and this growth depends on the incubation time and the amount of synthetic hydroxyapatite introduced into the composites as a cross-linking agent. This property has been studied by SEM, XRD, and FT-IR.

In concordance with the results of this work, we also propose that biocomposites may be used as potential drug delivery systems for analgesics, anti-inflammatories, and/or antibiotics, because of their capability to change from amorphous state to liquid crystal phases inside the composites, which can be modulated depending on the physiological pH values and ionic strength conditions. In this context, we demonstrated that the appearance of liquid crystal structures was not enough to keep these materials in a stable form, and for this reason, a portion of synthesized hydroxyapatite contributes to maintaining their integrity providing Ca^{2+} ions to their structure when pH value decreases. The decrease of biocomposites' stiffness at physiological pH is an important factor because the fluids and cells that reside in the zone of injury, capable of developing low pH conditions, can interact with these composites and reinforce their resistance thought internal gelation.

However, in addition to nano-hydroxyapatite, another source of Ca^{2+} ions is needed to maintain the structure of these composites (demonstrated by dissolution test) so as to be used as a potential inclusion in a live tissue.

In addition to these promising features, biocomposites show a pH-dependent behavior which presents encouraging previous results that should be corroborated through in vitro and in vivo studies to achieve an improvement in treatments for filling in bone injuries or illness-bone states.

Financial funding and acknowledgements The authors acknowledge the support from Universidad Nacional del Sur (PGI 24/Q064) and Concejo Nacional de Investigaciones Científicas y Técnicas de la República Argentina (CONICET, PIP 11220130100100CO). Paula Messina and Luciano Benedini are researchers of CONICET.

Compliance with ethical standards

Conflict of interest The authors declare that they have no conflicts of interest.

References

1. Dimitriou R, Mataliotakis GI, Angoules AG, et al. (2011) Complications following autologous bone graft harvesting from the iliac crest and using the RIA: a systematic review. Injury 42: S3–S15. https://doi.org/10.1016/j.injury.2011.06.015
2. Giannoudis PV, Dinopoulos H, Tsiridis E (2005) Bone substitutes: an update. Injury 36:S20–S27. https://doi.org/10.1016/j.injury.2005.07.029
3. D'Elía NL, Mathieu C, Hoemann CD, et al. (2015) Bone-repair properties of biodegradable hydroxyapatite nano-rod superstructures. Nano 7:18751–18762. https://doi.org/10.1039/C5NR04850H
4. Tautzenberger A, Kovtun I (2012) Nanoparticles and their potential for application in bone. Int J Nanomedicine 7:4545–4557. https://doi.org/10.2147/IJN.S34127
5. D'Elía NL, Gravina AN, Ruso JM, et al. (2013) Manipulating the bioactivity of hydroxyapatite nano-rods structured networks: effects on mineral coating morphology and growth kinetic. Biochim Biophys Acta - Gen Subj 1830:5014–5026. https://doi.org/10.1016/j.bbagen.2013.07.020
6. Cai Y, Yu J, Kundu SC, Yao J (2016) Multifunctional nano-hydroxyapatite and alginate/gelatin based sticky gel composites for potential bone regeneration. Mater Chem Phys 181:4–10. https://doi.org/10.1016/j.matchemphys.2016.06.053
7. Wei G, Ma PX (2004) Structure and properties of nano-hydroxyapatite/polymer composite scaffolds for bone tissue engineering. Biomaterials 25:4749–4757. https://doi.org/10.1016/j.biomaterials.2003.12.005
8. Kokubo T, Hanakawa M, Kawashita M, et al. (2004) Apatite deposition on calcium alginate fibres in simulated body fluid. J Ceram Soc Jpn 112:363–367. https://doi.org/10.2109/jcersj.112.363

9. Clarke B (2008) Normal bone anatomy and physiology. Clin J Am Soc Nephrol 3(Suppl 3):S131–S139. https://doi.org/10.2215/CJN.04151206
10. Lin H-R, Yeh Y-J (2004) Porous alginate/hydroxyapatite composite scaffolds for bone tissue engineering: preparation, characterization, andin vitro studies. J Biomed Mater Res 71B:52–65. https://doi.org/10.1002/jbm.b.30065
11. Ilie A, Ghițulică C, Andronescu E, et al. (2015) New composite materials based on alginate and hydroxyapatite as potential carriers for ascorbic acid. Int J Pharm 510:501–507. https://doi.org/10.1016/j.ijpharm.2016.01.025
12. Zhang J, Wang Q, Wang A (2010) In situ generation of sodium alginate/hydroxyapatite nanocomposite beads as drug-controlled release matrices. Acta Biomater 6:445–454. https://doi.org/10.1016/j.actbio.2009.07.001
13. Rwei SP, Nguyen TA (2015) Formation of liquid crystals and behavior of LCST upon addition of xanthan gum (XG) to hydroxypropyl cellulose (HPC) solutions. Cellulose 22:53–61. https://doi.org/10.1007/s10570-014-0469-y
14. Rwei SP, Nguyen TA, Chien-Jung Lee J, Chiang WY (2015) Liquid crystal formation and rheological study in aqueous blends of xanthan/acacia gum. Food Hydrocoll 46:52–58. https://doi.org/10.1016/j.foodhyd.2014.12.013
15. Quirolo ZB, Benedini LA, Sequeira MA, et al. (2014) Understanding recognition and self-assembly in biology using the chemist's toolbox. Insight into medicinal chemistry. Curr Top Med Chem 14:730–739. https://doi.org/10.2174/1568026614666140118220825
16. Melville AJ, Rodríguez-Lorenzo LM, Forsythe JS (2008) Effects of calcination temperature on the drug delivery behaviour of ibuprofen from hydroxyapatite powders. J Mater Sci Mater Med 19:1187–1195. https://doi.org/10.1007/s10856-007-3185-4
17. Nayak A, Laha B, Sen K (2011) Development of hydroxyapatite-ciprofloxacin bone-implants using "quality by design". Acta Pharma 61:25–36. https://doi.org/10.2478/v10007-011-0002-x
18. Öztürk E, Agalar C, Keçeci K, Denkbaş EB (2006) Preparation and characterization of ciprofloxacin-loaded alginate/chitosan sponge as a wound dressing material. J Appl Polym Sci 101:1602–1609. https://doi.org/10.1002/app.23563
19. Dong Z, Wang Q, Du Y (2006) Alginate/gelatin blend films and their properties for drug controlled release. J Memb Sci 280:37–44. https://doi.org/10.1016/j.memsci.2006.01.002
20. Islan GA, Mukherjee A, Castro GR (2015) Development of biopolymer nanocomposite for silver nanoparticles and ciprofloxacin controlled release. Int J Biol Macromol 72:740–750. https://doi.org/10.1016/j.ijbiomac.2014.09.020
21. Devanand Venkatasubbu G, Ramasamy S, Ramakrishnan V, Kumar J (2011) Hydroxyapatite-alginate nanocomposite as drug delivery matrix for sustained release of ciprofloxacin. J Biomed Nanotechnol 7:759–767. https://doi.org/10.1166/jbn.2011.1350
22. Salomonsen T, Jensen HM, Larsen FH, et al. (2009) Alginate monomer composition studied by solution- and solid-state NMR—a comparative chemometric study. Food Hydrocoll 23:1579–1586. https://doi.org/10.1016/j.foodhyd.2008.11.009
23. Rhim J-W (2004) Physical and mechanical properties of water resistant sodium alginate films. LWT - Food Sci Technol 37:323–330. https://doi.org/10.1016/j.lwt.2003.09.008
24. Kokubo T, Hanakawa M, Kawashita M, et al. (2004) Apatite-forming ability of alginate fibers treated with calcium hydroxide solution. J Mater Sci Mater Med 15:1007–1012. https://doi.org/10.1023/B:JMSM.0000042686.44977.81
25. Kokubo T, Kushitani H, Sakka S, et al (1990) Solutions able to reproduce in vivo surface-structure changes in bioactive glass-ceramic A-W3. J Biomed Mat Res 24:721–734. https://doi.org/10.1002/jbm.820240607
26. Padmanabhan SK, Balakrishnan A, Chu MC, et al. (2009) Sol-gel synthesis and characterization of hydroxyapatite nanorods. Particuology 7:466–470. https://doi.org/10.1016/j.partic.2009.06.008
27. Sangeetha K, Thamizhavel A, Girija EK (2013) Effect of gelatin on the in situ formation of alginate/hydroxyapatite nanocomposite. Mater Lett 91:27–30. https://doi.org/10.1016/j.matlet.2012.09.054
28. Xie M, Olderoy M, Andreassen JP, et al. (2010) Alginate-controlled formation of nanoscale calcium carbonate and hydroxyapatite mineral phase within hydrogel networks. Acta Biomater 6:3665–3675. https://doi.org/10.1016/j.actbio.2010.03.034
29. Pleshko N, Boskey A, Mendelsohn R (1991) Novel infrared spectroscopic method for the determination of crystallinity of hydroxyapatite minerals. Biophys J 60:786–793. https://doi.org/10.1016/S0006-3495(91)82113-0
30. Ruso JM, Verdinelli V, Hassan N, et al. (2013) Enhancing CaP biomimetic growth on TiO 2 cuboids nanoparticles via highly reactive facets. Langmuir 29:2350–2358. https://doi.org/10.1021/la305080x
31. Zhang S (2013) Hydroxyapatite coatings for biomedical applications. CRC Press Taylor and Francis Group, London,
32. Andersen T, Strand BL, Formo K, et al (2012) Alginates as biomaterials in tissue engineering In: Rauter AP (ed). Carbohydrate Chemistry: Chemical and Biological Approaches. The Royal Society of Chemistry 37, Cambridge, pp 227–258
33. Xu JB, Bartley JP, Johnson RA (2003) Preparation and characterization of alginate hydrogel membranes crosslinked using a water-soluble carbodiimide. J Appl Polym Sci 90:747–753. https://doi.org/10.1002/app.12713
34. Topuz F, Henke A, Richtering W, Groll J (2012) Magnesium ions and alginate do form hydrogels: a rheological study. Soft Matter 8:4877–4881. https://doi.org/10.1039/c2sm07465f
35. Melvik JE, Dornish M (2004) Fundamentals of cell immobilisation biotechnology. Fundam Cell Immobil Biotechnol. https://doi.org/10.1007/978-94-017-1638-3
36. Ingar Draget K, Ostgaard K, Smidsrod O (1990) Homogeneous alginate gels: a technical approach. Carbohydr Polym 14:159–178. https://doi.org/10.1016/0144-8617(90)90028-Q
37. Turco G, Marsich E, Bellomo F, et al (2009) Alginate/hydroxyapatite biocomposite for bone ingrowth: A Trabecular Structure With High And Isotropic Connectivity. Biomacromol 10:1575–1583. https://doi.org/10.1021/bm900154b
38. Reis CP, Ribeiro AJ, Neufeld RJ, V F (2006) Alginate microparticles as novel carrier for oral insulin delivery. Biotechnol Bioeng 96:977–989
39. Benavides S, Villalobos-Carvajal R, Reyes JE (2012) Physical, mechanical and antibacterial properties of alginate film: effect of the crosslinking degree and oregano essential oil concentration. J Food Eng 110:232–239. https://doi.org/10.1016/j.jfoodeng.2011.05.023
40. Haug AL, Larsen BS (1963) The degradation of alginates at different pH values. Acta Chem Scand 17(5):1466–1468. https://doi.org/10.3891/acta.chem.scand.17-1466
41. Williams PA, Phillips GO (2004) Gums and stabilisers for the food industry 12. The royal society of chemistry, thomas graham house, science park, milton road, Cambridge. https://doi.org/10.1039/9781847551214
42. Nakamura K, Hatakeyama T, Hatakeyama H (1991) Formation of the glassy state and mesophase in the water–sodium alginate system. Polym J 23:253–258. https://doi.org/10.1295/polymj.23.253
43. Ureña-Benavides EE, Ao G, Davis VA, Kitchens CL (2011) Rheology and phase behavior of lyotropic cellulose nanocrystal suspensions. Macromolecules 44:8990–8998. https://doi.org/10.1021/ma201649f
44. Ureña-Benavides EE, Brown PJ, Kitchens CL (2010) Effect of jet stretch and particle load on cellulose nanocrystal-alginate

nanocomposite fibers. Langmuir 26:14263–14270. https://doi.org/10.1021/la102216v

45. Desplanques S, Grisel M, Malhiac C, Renou F (2014) Stabilizing effect of acacia gum on the xanthan helical conformation in aqueous solution. Food Hydrocoll 35:181–188. https://doi.org/10.1016/j.foodhyd.2013.05.009
46. Lee KY, M DJ (2012) Alginate: properties and biomedical applications. Prog Polym Sci 37:106–126. https://doi.org/10.1016/j.progpolymsci.2011.06.003.Alginate
47. Grant GT, Morris ER, Rees DA, et al. (1973) Biological interactions between polysaccharides and divalent cations: the egg-box model. FEBS Lett 32:195–198. https://doi.org/10.1016/0014-5793(73)80770-7
48. Wolnik A, Albertin L, Charlier L, Mazeau K (2013) Probing the helical forms of Ca2+-guluronan junction zones in alginate gels by molecular dynamics 1: duplexes. Biopolymers 99:562–571. https://doi.org/10.1002/bip.22216
49. Sugawara E, Nikaido H (2009) Alginates: biology and applications. Antimicrob Agents Chemother. https://doi.org/10.1007/978-3-540-92679-5
50. Zhang C, Li C, Huang S, et al. (2010) Self-activated luminescent and mesoporous strontium hydroxyapatite nanorods for drug delivery. Biomaterials 31:3374–3383. https://doi.org/10.1016/j.biomaterials.2010.01.044
51. Venkatesan J, Nithya R, Sudha PN, Kim S-K (2014) Chapter four—role of alginate in bone tissue engineering. Adv Food Nutr Res 73. https://doi.org/10.1016/B978-0-12-800268-1.00004-4
52. Benedini L, Messina PV, Palma SD, et al. (2012) The ascorbyl palmitate-polyethyleneglycol 400-water system phase behavior. Colloids Surf B Biointerfaces 89:265–270. https://doi.org/10.1016/j.colsurfb.2011.09.030
53. Ullio Gamboa GV, Benedini LA, Schulz PC, Allemandi DA (2016) Phase behavior of ascorbyl palmitate coagels loaded with oligonucleotides as a new carrier for vaccine adjuvants. J Surfactant Deterg 19:747–757. https://doi.org/10.1007/s11743-016-1816-9